

Projected Sliced Wasserstein Autoencoder-based Hyperspectral Images Anomaly Detection

Yurong Chen, *Member, IEEE*, Hui Zhang, *Member, IEEE*, Yaonan Wang,
Q. M. Jonathan Wu, *Senior Member, IEEE*, Yimin Yang, *Senior Member, IEEE*

Abstract—Anomaly detection (AD) has been an active research area in various domains. Yet, the increasing data scale, complexity, and dimension turn the traditional methods into challenging. Recently, the deep generative model, such as the variational autoencoder (VAE), has sparked a renewed interest in the AD problem. However, the probability distribution divergence used as the regularization is too strong, which causes the model cannot capture the manifold of the true data. In this paper, we propose the Projected Sliced Wasserstein (PSW) autoencoder-based anomaly detection method. Rooted in the optimal transportation, the PSW distance is a weaker distribution measure compared with f -divergence. In particular, the computation-friendly eigen-decomposition method is leveraged to find the principal component for slicing the high-dimensional data. In this case, the Wasserstein distance can be calculated with the closed-form, even the prior distribution is not Gaussian. Comprehensive experiments conducted on various real-world hyperspectral anomaly detection benchmarks demonstrate the superior performance of the proposed method.

Index Terms—Anomaly Detection, Variational Inference, Representation Learning, Hyperspectral Images.

I. INTRODUCTION

A. Background

ANOMALY detection (AD) or outlier detection refers to identifying the observation that deviates from the expected pattern. The first formal definitions of the anomaly, so-called ‘discordant observations’, can date back to the 19th [1]. Spanning more than one hundred years, it has been attracting researchers’ attention a lot due to its wide usage in diverse applications, such as hyperspectral imaging [2], intelligent plant [3]. While human beings are born with the

capability of the novelty perception [4], anomaly detection is enormously difficult for machine learning methods. One of the key challenges is that we cannot access the prior knowledge of outliers. This incurs labeled anomalous data is often non-existent. When available, the occurrence chance of the anomaly is extremely lower than the normal samples that it is insufficient to fully modelling all notions of outliers [5]. These traits motivate researchers to treat outlier detection as a one-class classification (OCC), but a binary classification task.

B. Motivation and Problem Setting

There has been a surge of work focused on applying deep learning to OCC algorithms [6][7][8]. The semi-supervised autoencoder (AE) is one of the most prevalent frameworks among them [3]. The philosophy is that regularities of the normal pattern can be captured into a compact latent variable [9]. As a result, the latent feature of the normal sample can be used to generate the original data. Conversely, the network cannot reconstruct the input anomaly data well with its latent representation. Moreover, there are some improvements for AE-based hyperspectral anomaly detection. For example, Zhao et al. [10] propose the stacked spectral-spatial AEs method that leverages the spectral and spatial feature. The data manifold constrained AE is introduced in [11], which encourages the representation to keep the local information of the hyperspectral data. Zhang et al. [12] design a full-automatic AD-based anomaly detection network that does not require pre-processing or post-processing.

The idea of the autoencoder-based AD is theoretically elegant, however, its performance is not satisfactory. One main challenge is that the AE sometimes “generalizes” so well [13] that the anomaly can also be reconstructed well. For this reason, it is hard to threshold the reconstruction error between normal samples and anomalies. Researchers tend to attribute this failure to the autoencoder cannot capture the manifold of the true normal data [14]. Therefore, the Variational autoencoder (VAE) [15] based AD explicitly fits the model to learn the distribution of the normal data, while the out-of-distribution sample can be viewed as the outlier. The objective function of the VAE consists of the reconstruction loss and the divergence as the regularization. The former ensures the majority of inputs’ information can be encoded, while the latter encourages the model to ignore the trivial features. VAE has made remarkable progress in learning high-dimensional distributions, however, applying it in practical abnormality detection is still an ill-posed problem. Here, we

This work was supported in part by the National Key Research and Development Program of China under Grant 2018YFB1308200; in part by the National Natural Science Foundation of China under Grant 61971071, Grant 62027810, and Grant 62133005; in part by the Hunan Science Fund for Distinguished Young Scholars under Grant 2021JJ10025; in part by the Changsha Science and Technology Major Project under Grant kh2003026; in part by the Joint Open Foundation of State Key Laboratory of Robotics under Grant 2021-KF-22-17; in part by the China University Industry-University-Research Innovation Fund under Grant 2020HYA06006; Corresponding author: Hui Zhang, Yaonan Wang.

Yurong Chen, Hui Zhang, and Yaonan Wang are with the National Engineering Laboratory of Robot Visual Perception and Control Technology, School of Robotics, Hunan University, Changsha 410082, Hunan, China (e-mail: chenyrong1998@outlook.com; zhanghuihy@126.com; yaonan@hnu.edu.cn).

Q. M. J. Wu is with the Department of Electrical and Computer Engineering, University of Windsor, Windsor, Ontario, N9B3P4 Canada (e-mail: jwu@uwindsor.ca).

Y. Yang is with the Department of Computer Science, Lakehead University, Ontario, P7B 5E1, Canada, also with the Vector Institute, Toronto, M5G 1M1, Canada. (e-mail: yyang48@lakeheadu.ca).

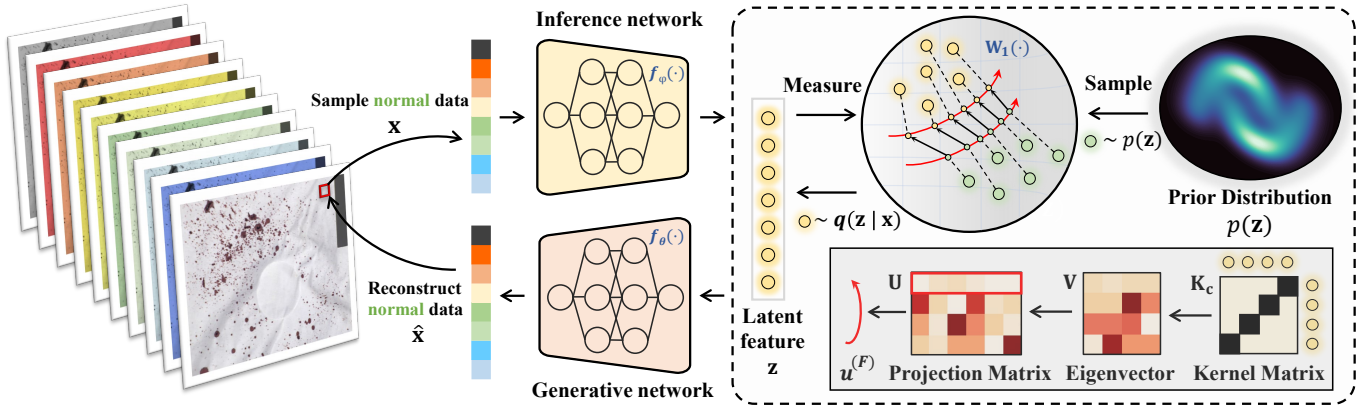


Fig. 1: Illustration about the training phase of the proposed projected sliced Wasserstein (PSW) autoencoder-based automatic hyperspectral outlier detection framework.

find the sub-par and unstable anomaly detection accuracy is highly related to the regularization.

The common information theoretic dissimilarity metric (f -divergence), as the regularization term, is a strong notion of distance. It calculates the density ratio between distributions, often max out (i.e. provides useless gradients) [16]. Therefore, the regularization is “over-optimized” and the reconstruction loss is “under-optimized”. As a consequence, the autoencoder network cannot reconstruct its input. The reconstruction errors of both normal and abnormal samples are high. The simplistic prior distribution (e.g. isotropic Gaussian) poses another challenge for applying the VAE to anomaly detection. In practical hyperspectral anomaly detection tasks, the normal items always belong to multi-classes and each owns a different spectrum pattern. The standard normal distribution for the prior leads to the overly smooth reconstruction [17]. Utilizing the mixture prior distribution can be an intuitive method [18], however, does not allow for closed-form optimization.

The Wasserstein-based autoencoder is proposed to alleviate this dilemma [16]. As opposed to the KL divergence, the Wasserstein distance, as a weak probability measure, has attracted a lot of interest in the learning community [16]. Moreover, the sliced Wasserstein distance introduces the Random Variable Transformation (RVT) to factorize high-dimensional distributions into one-dimensional marginal yet maintains the topology of the Wasserstein distance [18]. Yet, the number of slicing is the key hyper-parameter. A small number of projections is computationally effective, however, it can be short of capturing meaningful distribution information, vice versa. The dilemma could be traced to the uncertainty of stochastic slicing. In addition, the non-linear data may be collapsed after the linear projection. Therefore, a generalized deep generative model for the practical AD problem is needed.

C. Contribution

Firstly, the objective of the VAE, i.e. evidence lower bound (ELBO), is derived based on the variational inference. We show that the objective can be calculated as the closed-form under the Gaussian distribution assumption. Moreover, we provide the analysis of the objective from the information

theory point of view. The mutual information between the input and its latent variable is investigated. Under the mild assumption, minimizing the KL divergence of ELBO would decrease the MI (or correlation). In other words, the input and the latent variable would become more independent when the KL divergence is ‘well’ optimized. Motivated by the β -VAE [19], we empirically study the effect of the weight of the divergence term on anomaly detection. With a smaller hyper-parameter β (the weight of the divergence), the VAE can perform the AD task. However, the performance is sensitive to β , and tuning it is a trivial and troublesome process.

Secondly, this paper proposes the projected sliced Wasserstein (PSW) autoencoder-based full automatic hyperspectral outlier detection framework, as shown in Fig. 1. Rooted in the optimal transportation theory, the PSW is a weaker notion of distribution distances, which is more suitable as the regularization term. Compared with the random transformation, the projected slicing method aims to find the meaningful one-dimensional marginal. Inspired by the kernel trick, we construct the kernel matrix. Then, a fast and stable eigen-decomposition method [20] is leveraged to find the transforming matrix on the kernel matrix. The slicing is performed via projecting the high-dimensional latent features into the first principal subspace. With the sliced one-dimensional data, the Wasserstein can be calculated.

Moreover, note that the prior distribution plays a crucial role in mediating between the variational encoder and the generative decoder [21]. The KL divergence of the vanilla VAE can be calculated with the closed-form under the Gaussian or Bernoulli prior assumption [15]. These simplistic distributions could lead the feature to be less discriminative, therefore, the model has poor generative capability. Owing to the proposed projected sliced Wasserstein distance as the regularizer, the discrepancy between the inference distributions and complex priors can be estimated with the closed-form. In this paper, we incorporate richer, multi-modal priors into the autoencoder to encourage the model to be more generative. Therefore, the model has the better capability to reconstruct the sophisticated and complex background hyperspectral data.

Finally, our contributions can be summarized as follows:

- We theoretically and empirically show the instability of the VAE-based anomaly detection is related to the regularization, i.e. KL divergence.
- We propose the projected sliced Wasserstein distance to deal with problems of the strong notion of distances. In addition, it is more computation-effective.
- The closed-form optimization of various, multi-modal prior distributions is implemented to increase the model generative capability.
- Comprehensive experiments, conducted on several hyperspectral anomaly detection benchmarks, show the superior performance of our method.

II. RELATED WORK

Recent one-class classification studies fall into three main types: representation-based methods, statistical techniques, and deep learning-based algorithms.

A. Representation-based Anomaly Detection

The assumption of representation-based methods is that the background instances can be decomposed as a set of bases, while anomalies cannot be represented well. For example, Principal component analysis (PCA) describes the normal data with the principal components of the subspace [22]. The gist is that the anomaly should exhibit more reconstruction error than a normal one when applying inverting PCA transform. Collaborative-representation-based detector (CRD) [23] leverages the local spatial information and assumes that the background pixel can be represented by the linear combination of its neighborhoods while outliers cannot. Yang et al. utilize the neighbors' spatial homogeneity into the total variation (TV) method [24]. Sparse representation-based method [25] has demonstrated the superior performance. There is a tendency to develop the low-rank and sparse decomposition model (LSDM) [26][27]. They aim to process the data into a low-rank matrix that is used to represent the background and a sparse matrix to denote the anomaly component. However, the matrix decomposition technique and their transductive learning-based idea are challenged by nowadays large-scale data. Moreover, Isolation forest (IForest) [28] uses the training normal data to build trees, then the test point is passed through trees for anomaly scoring. Local outlier factor (LOF) [29] assigns the degree based on how isolated the data is with respect to the local neighborhood. FastABOD [30] leverages angle based distance to mitigating the high dimension problem of LOF. Average kNN [31] uses the average distance to k nearest neighbors as the outlier score. The hybrid sparsity and statistics detector (HSSD) for anomaly detection in hyperspectral imagery is proposed in [32].

B. Statistics-based Anomaly Detection

The statistics-based anomaly detection algorithms have been developing since the capability of inductive learning. The Reed–Xiaoli (RX) algorithm [33] is a landmark anomaly detection for many areas. It hypothesizes the data as normal distribution and then estimates its mean vector and covariance

matrix. The anomaly score is performed as the Mahalanobis distance between the test pixel and background. Besides that, there are some variants based on the RX algorithm, such as the linear filter-based RX detector [34] that can estimate background statistical characteristics more precise that more robust to the noise; The local RX detector (LRX) [35] utilizes the local statistics to improve detection performance. DWT-RX combines the discrete wavelet transform [36]. However, these methods assume that the training data follows a normal distribution, which may violate or limit the real data characteristic. Moreover, One-class SVM (OCSVM) [37] introduces the idea of learning to find the hyper-plane furthest away from the origin, in which the anomaly exists in the negative half-space of the hyper-plane. Notwithstanding, these methods cannot achieve satisfying performance on high-dimensional caused by the curse of dimensionality and no feature extraction stage. Moreover, their statistical assumption on the data domain is hampered by the complex characteristic of the background. Copula-based outlier detection (COPOD) [38] modelling multivariate data distribution and uses p-value for anomaly detection.

C. Deep learning-based Anomaly Detection

There are numerous deep learning methods in the literature [39]. We focus on the autoencoder-based outlier detection. Some related algorithms are discussed in the introduction. Here, we would like to provide relevant knowledge about **variational inference**. Instead of modelling the density of background in the data domain, ones can resort to it in the latent space. Inference amounts to conditioning on data and calculating the posterior distribution $p(\mathbf{z}|\mathbf{x})$. According to the Bayesian Theorem, the posterior can be computed as: $p(\mathbf{z}|\mathbf{x}) = \frac{p(\mathbf{x}|\mathbf{z})p(\mathbf{z})}{p(\mathbf{x})}$, where the marginal distribution $p(\mathbf{x}) = \int p(\mathbf{x}|\mathbf{z})p(\mathbf{z})d\mathbf{z}$. Due the integral operation, the calculating of $p(\mathbf{x})$ is always intractable. Although the Markov chain Monte Carlo (MCMC) sampling strategy is a tool [40], there are problems for which we cannot easily use it, such as when the scale of the data set is large. In contrast, the gist of variational inference is to approximate the intractable posterior to the given density. The KL divergence can be utilized for measuring the difference between the true posterior $p(\mathbf{z}|\mathbf{x})$ and the variational posterior $q(\mathbf{z}|\mathbf{x})$:

$$\begin{aligned}
 D_{KL}(q(\mathbf{z}|\mathbf{x}) || p(\mathbf{z}|\mathbf{x})) &= \int q(\mathbf{z}|\mathbf{x}) \log \frac{q(\mathbf{z}|\mathbf{x})}{p(\mathbf{z}|\mathbf{x})} d\mathbf{z} \\
 &= \int q(\mathbf{z}|\mathbf{x}) \log \frac{q(\mathbf{z}|\mathbf{x})p(\mathbf{x})}{p(\mathbf{x}|\mathbf{z})p(\mathbf{z})} d\mathbf{z} \\
 &= \underbrace{\int q(\mathbf{z}|\mathbf{x}) \log \frac{q(\mathbf{z}|\mathbf{x})}{p(\mathbf{z})} d\mathbf{z}}_{D_{KL}(q(\mathbf{z}|\mathbf{x}) || p(\mathbf{z}))} - \int q(\mathbf{z}|\mathbf{x}) \log \frac{p(\mathbf{x}|\mathbf{z})}{p(\mathbf{x})} d\mathbf{z}.
 \end{aligned} \tag{1}$$

This can be wrote as:

$$\begin{aligned}
 D_{KL}(q(\mathbf{z}|\mathbf{x}) || p(\mathbf{z}|\mathbf{x})) &= D_{KL}(q(\mathbf{z}|\mathbf{x}) || p(\mathbf{z})) \\
 &\quad - \int q(\mathbf{z}|\mathbf{x}) \log p(\mathbf{x}|\mathbf{z}) d\mathbf{z} + \int q(\mathbf{z}|\mathbf{x}) \log p(\mathbf{x}) d\mathbf{z}.
 \end{aligned} \tag{2}$$

TABLE I: Notions Definition

| Notion | Definition |
|----------------------------|--|
| \mathbf{x} | The hyperspectral data point; |
| \mathbf{z} | The latent feature of the hyperspectral data point; |
| \mathcal{X} | Data space; |
| \mathcal{Z} | Latent feature space; |
| $p_{gt}(\mathbf{x})$ | Distribution of the normal data; |
| $p_{\theta}(\mathbf{x})$ | Modelling distribution of the normal data; |
| $p(\mathbf{z} \mathbf{x})$ | True posterior distribution of the normal data; |
| $p(\mathbf{x} \mathbf{z})$ | Likelihood distribution of the normal data; |
| $q(\mathbf{z} \mathbf{x})$ | Variational posterior distribution of the normal data; |
| $p(\mathbf{z})$ | Prior distribution of the latent feature; |
| $f_{\varphi}(\cdot)$ | Inference network, i.e. encoder; |
| $f_{\theta}(\cdot)$ | Generative network, i.e. decoder; |
| N | Number of data points; |
| B | Number of hyperspectral bands; |
| M | Dimensions of the latent feature; |
| ϵ | The threshold value for classifying anomalies; |

The sum of $q(\mathbf{z}|\mathbf{x})$ equals to one ($\int q(\mathbf{z}|\mathbf{x})d\mathbf{z} = 1$), so that $\int q(\mathbf{z}|\mathbf{x})\log p(\mathbf{x})d\mathbf{z} = \log p(\mathbf{x})$. Given a data point, $\log p(\mathbf{x})$ is a constant, therefore we move it to the left hand side:

$$\log p(\mathbf{x}) = D_{KL}(q(\mathbf{z}|\mathbf{x}) \parallel p(\mathbf{z}|\mathbf{x})) - D_{KL}(q(\mathbf{z}|\mathbf{x}) \parallel p(\mathbf{z})) + \int q(\mathbf{z}|\mathbf{x})\log p(\mathbf{x}|\mathbf{z})d\mathbf{z}. \quad (3)$$

In the end, variational inference turns the inference problem into an optimization problem, which would like to minimize the $D_{KL}(q(\mathbf{z}|\mathbf{x}) \parallel p(\mathbf{z}|\mathbf{x}))$, as equivalent to maximize the Evidence Lower Bound (ELBO)

$$\mathcal{L}_{ELBO} := \mathbb{E}_{q(\mathbf{z}|\mathbf{x})}[\log p(\mathbf{x}|\mathbf{z})] - D_{KL}(q(\mathbf{z}|\mathbf{x}) \parallel p(\mathbf{z})). \quad (4)$$

The variational distribution is close to the true posterior when maximizing the accumulated log posterior predictive probability and minimizing the KL divergence between the amortized distribution and the prior.

III. METHOD

In this section, we formulate the notion and problem of hyperspectral anomaly detection in part A, firstly. Then, we discuss the VAE-based anomaly detection method and its shortcomings in part B. In the end, the detail of the proposed projected sliced Wasserstein autoencoder anomaly detection framework is provided in section III.C.

A. Notion and Problem Formulation

This work considers the hyperspectral anomaly screening under a semi-supervised setting, i.e. only the normal cases are available during the training phase. Suppose the normal data follows a ground truth distribution $p_{gt}(\mathbf{x})$ on the data domain \mathcal{X} . We can collecting i.i.d samples from $p_{gt}(\mathbf{x})$ to create a training set $D = \{\mathbf{x}_1, \dots, \mathbf{x}_i, \dots, \mathbf{x}_N\}$ where $\mathbf{x}_i \in \mathbb{R}^{B \times 1}$ with the band number of B). The key of maximum likelihood model-based anomaly detection is to learn a probabilistic model $p_{\theta}(\mathbf{x})$ parameterized by θ . The objective is to maximize the likelihood of the joint distribution $p_{\theta}(\mathbf{x}_1, \dots, \mathbf{x}_N) = \prod_{i=1}^N p_{\theta}(\mathbf{x}_i)$. In general, we maximize the log-likelihood for numerical stability $\log p_{\theta}(\mathbf{x}_1, \dots, \mathbf{x}_N) = \sum_{i=1}^N \log p_{\theta}(\mathbf{x}_i)$.

Let \mathcal{Z} be the latent space, and $\mathbf{z}_i \in \mathbb{R}^{M \times 1}$ is the corresponding latent features of \mathbf{x}_i , where M is the dimension of

the latent feature. Based on the philosophy of generative model [15], we resort to modelling the posterior distribution $p(\mathbf{z}|\mathbf{x})$, which is the conditional distribution of the normal latent code. It is realized with a **probabilistic** inference network $f_{\varphi}(\cdot) : \mathcal{X} \rightarrow \mathcal{Z}$. In addition, a **deterministic** outlier estimation function $f_{\theta}(\cdot) : \mathcal{Z} \rightarrow \mathcal{X}$ is utilized to score the anomaly. $f_{\varphi}(\cdot)$ and $f_{\theta}(\cdot)$ can be parameterized by two neural network, often known as the encoder and decoder network. In most anomaly detection cases, the pretext task is to reconstruct the input data \mathbf{x}_i via $f_{\varphi}(\cdot)$ and $f_{\theta}(\cdot)$:

$$\hat{\mathbf{x}}_i = f_{\theta}(f_{\varphi}(\mathbf{x}_i)). \quad (5)$$

Under the assumption that the true data distribution is captured by the model, the normal hyperspectral data can be reconstructed well, while the out-of-distribution outliers cannot. Anomalies recognition in the testing phase can be achieved by setting a threshold value ϵ of the L_n -reconstruction error:

$$\|\mathbf{x}_i, \hat{\mathbf{x}}_i\|_n = \|\mathbf{x}_i, f_{\theta}(f_{\varphi}(\mathbf{x}_i))\|_n \geq \epsilon \in \mathbb{R}. \quad (6)$$

B. β -Variational Autoencoder based AD

The essence of the VAE-based anomaly detection is to fit the normal data distribution by the neural network with introducing a latent variable \mathbf{z} . The VAE explicitly models the latent distribution, i.e. given a prior distribution $p(\mathbf{z})$, the posterior is directly approximated via minimizing their divergence [15]. In particular, with the analysis-synthesis idea in mind, the VAE consists of two neural networks: an inference network (encoder) $f_{\varphi}(\cdot) \subseteq q(\mathbf{z}|\mathbf{x})$ and a generative network (decoder) $f_{\theta}(\cdot) \subseteq p(\mathbf{x}|\mathbf{z})$. The inference network maps the data \mathbf{x} to the variable \mathbf{z} , which follows the variational distribution $q(\mathbf{z}|\mathbf{x})$. The decoder transforms the latent variable \mathbf{z} back to data \mathbf{x} . The two neural networks are jointly trained with the objective of variational inference (Eq. 6). Under the assumption that both the likelihood $p(\mathbf{x}|\mathbf{z})$ is Gaussian $\mathcal{N}(\mu_{\theta}(\mathbf{z}), \sigma_{\theta}^2(\mathbf{z}))$, the first term on the right hand side is derived to

$$\mathbb{E}_{q(\mathbf{z}|\mathbf{x})}[\log p(\mathbf{x}|\mathbf{z})] = \mathbb{E}_{q(\mathbf{z}|\mathbf{x})}\left[-\sum_{i=1}^N \frac{1}{2} \log 2\pi\sigma_{\theta}^2(\mathbf{z})_i - \frac{(\mathbf{x}_i - \mu_{\theta}(\mathbf{z})_i)^2}{2\sigma_{\theta}^2(\mathbf{z})_i}\right]. \quad (7)$$

In a simplified VAE, this term is relaxed as the negative mean square error (MSE)

$$-\frac{1}{n} \mathbb{E}_{\mathbf{x} \sim p_{gt}(\mathbf{x}), \mathbf{x} \sim q(\mathbf{z}|\mathbf{x})} [\|\mathbf{x} - \mu_{\theta}(\mathbf{z})\|_2^2]. \quad (8)$$

It can be understood as the negative reconstruction error between the input and the output of the decoder. Therefore, maximizing the evidence lower bound pushes the decoder to seeks to best reconstruct \mathbf{x} based on \mathbf{z} .

Using the standard isotropic multi-variate Gaussian as the prior $p(\mathbf{z}) = \mathcal{N}(0, \mathbf{I})$, the variational posterior distribution is a multi-variate Gaussian $p(\mathbf{z}|\mathbf{x}) = \mathcal{N}(\mu_{\varphi}(\mathbf{x}), \sigma_{\varphi}^2(\mathbf{x}))$. In this

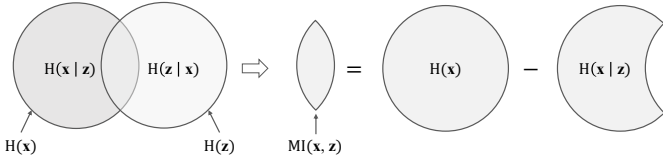


Fig. 2: The Venn-Diagram of the mutual information $MI(\mathbf{x}, \mathbf{z})$. When the $MI(\mathbf{x}, \mathbf{z})$ is small, the variable \mathbf{z} provides less information about the \mathbf{x} .

case, the second RHS (KL divergence) can be expressed as the closed-form:

$$D_{KL}(q(\mathbf{z}|\mathbf{x}) \parallel p(\mathbf{z})) = \frac{1}{2} \left[\|\mu_\varphi(\mathbf{x})\|_2^2 + \|\sigma_\varphi^2(\mathbf{x})\|_2^2 - \sum_{i=1}^F (\log \sigma_\varphi^2(\mathbf{x}) + 1) \right]. \quad (9)$$

For convenient implementation, the covariance is usually diagonal $diag(\sigma_\varphi^2(\mathbf{x}))$. Hence, given the input \mathbf{x} , the encoder outputs two vectors $\mu_\varphi(\mathbf{x}), \sigma_\varphi^2(\mathbf{x}) \in \mathbb{R}^M$. Thus, minimizing the KL divergence equals maximizing the ELBO. It encourages the encoder $f_\varphi(\cdot)$ to decrease $\|\mu_\varphi(\mathbf{x})\|$ and increase $\sigma_\varphi^2(\mathbf{x})$. After approximation, the stochastic sampling of \mathbf{z} from $q(\mathbf{z}|\mathbf{x})$ is implemented with a deterministic function via the re-parameterization trick:

$$\mathbf{z} = \mu_\varphi(\mathbf{x}) + \sigma_\varphi(\mathbf{x}) \odot \mathbf{u}, \quad (10)$$

where $\mathbf{u} \sim \mathcal{N}(0, \mathbf{I})$ and \odot signals the element-wise product.

In a nutshell, the objective of the vanilla VAE-based anomaly detection usually consists of two terms: the reconstruction loss $\mathcal{L}_{rec} = MSE$ (the negative of Eq. 8) and the regularization loss $\mathcal{L}_{reg} = D_{KL}$ (the negative of Eq. 9) i.e. $\mathcal{L}_{VAE} = \mathcal{L}_{rec} + \mathcal{L}_{reg}$. \mathcal{L}_{rec} encourages the encoder to learn more meaningful representations aspect with the input normal data, and \mathcal{L}_{reg} imposes a regularization to the model that pushes it to ignore other trivial features. However, optimization with \mathcal{L}_{VAE} is hard to achieve superior performance. As we talked about in the introduction section, \mathcal{L}_{reg} as a strong distance notion, often poses a difficult challenge in representation learning.

At first, we provide the theoretical analysis from the mutual information (MI) point of view, as illustrated in Fig. 2. We show that minimizing the \mathcal{L}_{reg} would decrease the MI between the input variable \mathbf{x} and the latent code \mathbf{z} . Based on the definition of the MI [41], the upper bound can be derived with introducing the variational distribution $q(\mathbf{z}|\mathbf{x})$:

$$\begin{aligned} MI(\mathbf{x}, \mathbf{z}) &= \mathbb{E}_{p(\mathbf{x}, \mathbf{z})} \left[\log \frac{p(\mathbf{z}|\mathbf{x})}{p(\mathbf{z})} \right] \\ &= \mathbb{E}_{p(\mathbf{x}, \mathbf{z})} \left[\log \frac{p(\mathbf{z}|\mathbf{x}) q(\mathbf{z}|\mathbf{x})}{q(\mathbf{z}|\mathbf{x}) p(\mathbf{z})} \right] \\ &= \mathbb{E}_{p(\mathbf{x}, \mathbf{z})} \left[\log \frac{p(\mathbf{z}|\mathbf{x})}{q(\mathbf{z}|\mathbf{x})} \right] - \mathbb{E}_{p(\mathbf{x}, \mathbf{z})} \left[\log \frac{p(\mathbf{z})}{q(\mathbf{z}|\mathbf{x})} \right] \\ &= \mathbb{E}_{p(\mathbf{x})} \left[D_{KL}(p(\mathbf{z}|\mathbf{x}) \parallel q(\mathbf{z}|\mathbf{x})) \right] \\ &\quad - D_{KL}(p(\mathbf{z}) \parallel q(\mathbf{z}|\mathbf{x})). \end{aligned} \quad (11)$$

Algorithm 1: The β -VAE based anomaly detection

Target:

- 1: Learn a network for modelling the distribution of input \mathbf{x} , which can well reconstruct the normal data \mathbf{x}_{nor} but the anomaly \mathbf{x}_{ano} ;
- 2: Manually find the optimal hyperparameter β .

Procedure:

Step 1: Initialize networks $f_\varphi(\cdot)$, $f_\theta(\cdot)$, and the coefficient β ;

Step 2: **while** not converged **do**

1: Randomly sample the normal data: $\mathbf{x} \sim p_{gt}(\mathbf{x})$;

2: Inference the posterior distribution of each data point \mathbf{x} via Eq. 10: $\mathbf{z} \sim q(\mathbf{z}|\mathbf{x}) = f_\varphi(\mathbf{x})$;

3: Calculate the KL divergence between the variational distribution and the prior distribution via Eq. 9: \mathcal{L}_{reg} ;

4: Generate (reconstruct) the input data: $\hat{\mathbf{x}} = f_\theta(\mathbf{z})$;

5: Calculate the reconstruction error: $\mathcal{L}_{rec} = \|\hat{\mathbf{x}} - \mathbf{x}\|_2^2$;

6: Δ Updates $f_\varphi(\cdot)$ and $f_\theta(\cdot)$ with $\mathcal{L}_{rec} + \beta \mathcal{L}_{reg}$;

end while

Step 3: Calculate the reconstruction error of test data: \mathcal{L}_{rec}^{Test} ;

Step 4: Set a threshold ϵ : $\hat{y}_{ano} = \{\mathcal{L}_{rec}^{Test} \geq \epsilon\}$;

Step 5: Change the hyperparameter β and repeat step 1-4.

Output: The best anomaly detection accuracy;

The parameter of networks $f_\varphi(\cdot)$, $f_\theta(\cdot)$;

The hyperparameter β .

Because of the non-negativity of KL divergence, the above equation is smaller than the first RHS term:

$$MI(\mathbf{x}, \mathbf{z}) \leq \underbrace{\mathbb{E}_{p(\mathbf{x})} \left[D_{KL}(p(\mathbf{z}|\mathbf{x}) \parallel q(\mathbf{z}|\mathbf{x})) \right]}_{\text{The upper bound of MI}}. \quad (12)$$

Let's recall the derivation of variational inference. Its' objective is to approximate the true posterior $p(\mathbf{z}|\mathbf{x})$. Although KL divergence is asymmetric, i.e.

$$D_{KL}(q(\mathbf{z}|\mathbf{x}) \parallel p(\mathbf{z}|\mathbf{x})) \neq D_{KL}(p(\mathbf{z}|\mathbf{x}) \parallel q(\mathbf{z}|\mathbf{x})), \quad (13)$$

minimizing the $D_{KL}(q(\mathbf{z}|\mathbf{x}) \parallel p(\mathbf{z}|\mathbf{x}))$ will push two distributions closer, which somehow decreases the $D_{KL}(p(\mathbf{z}|\mathbf{x}) \parallel q(\mathbf{z}|\mathbf{x}))$. If and only if $q(\mathbf{z}|\mathbf{x}) = p(\mathbf{z}|\mathbf{x})$, these two KL divergences equal to zero $D_{KL}(q(\mathbf{z}|\mathbf{x}) \parallel p(\mathbf{z}|\mathbf{x})) = D_{KL}(p(\mathbf{z}|\mathbf{x}) \parallel q(\mathbf{z}|\mathbf{x})) = 0$. As shown in Fig. 2 and Eq. 12, when the KL is well optimized, the $MI(\mathbf{x}, \mathbf{z})$ approaches to zero. It means that when we observed the latent feature \mathbf{z} , we cannot give any useful information about \mathbf{x} . This phenomenon is also called posterior collapsed [19] that the decoder ignores the representation and generates samples only based on the random noise. Thus, these challenges always turn the VAE-based anomaly detection into a delicate algorithm.

Recently, the β -VAE [19] introduces an adjustable hyperparameter β to balance the reconstruction fidelity \mathcal{L}_{rec} and the strong distribution approximation constraint \mathcal{L}_{reg} :

$$\begin{aligned} \mathcal{L}_{\beta\text{-VAE}} &= \mathcal{L}_{rec} + \beta \mathcal{L}_{reg} \\ &= \|\mathbf{x} - \mu_\theta(\mathbf{z})\|_2^2 - \beta D_{KL}(q(\mathbf{z}|\mathbf{x}) \parallel p(\mathbf{z})). \end{aligned} \quad (14)$$

It argues that \mathcal{L}_{reg} controls the emphasis on learning independent latent factors. The model is encouraged to capture a more disentangled latent representation of the data with $\beta > 1$. While the β -VAE shows superior performance in the representation learning task, there is little theoretically and

empirically analysis of the hyper-parameter β in the VAE-based anomaly detection. One of the main contributions of this paper is that we heuristically investigate the effect of β in the AD task. We uncover that the vanilla VAE ($\beta = 1$) cannot perform detecting the outliers, but the β -VAE can achieve a presentable AD performance when the β is a small coefficient e.g. $\beta < 1$. Different from disentangled representation learning, the basics of anomaly detection is to maintain the manifold of the normal data. Therefore, a mild regularization is more beneficial. In addition, we empirically study the various β from the accuracy of anomaly detection and posterior distribution point of view, in the later section.

C. Projected Sliced Wasserstein Autoencoder based AD

In the last section, we show the flowchart of the β -VAE based anomaly detection. Moreover, the theoretical analysis of why this framework cannot perform AD is provided. In this part, we would illustrate the proposed projected sliced Wasserstein (PSW) autoencoder-based outlier detection algorithm. Rooted in optimal transport [16], the p -Wasserstein distance between two distribution is:

$$W_p(p(\mathbf{z}), q(\mathbf{z})) = \inf_{\gamma \in \Pi(p(\mathbf{z}), q(\mathbf{z}))} \mathbb{E}_{(\tilde{\mathbf{z}}, \mathbf{z}) \sim \gamma} [d(\tilde{\mathbf{z}}, \mathbf{z})]^\frac{1}{p}, \quad (15)$$

where $\Pi(p(\mathbf{z}), q(\mathbf{z}))$ represents the family of all joint distributions (transport maps in the optimal transport); $p(\mathbf{z}), q(\mathbf{z})$ is the marginal density of $\tilde{\mathbf{z}}, \mathbf{z}$, individually; $d(\cdot)$ is any measurable cost function. In general, the Wasserstein distance does not allow closed-form calculation. One important exception is the case where $p = 1$, $\mathcal{Z} = \mathbb{R}$, and $d(\tilde{\mathbf{z}}, \mathbf{z}) = \|\tilde{\mathbf{z}} - \mathbf{z}\|_2$. The explicit formula holds:

$$W_1(p(\mathbf{z}), q(\mathbf{z})) = \sum_{i=1}^M \|F_p(i) - F_q(i)\|_2^2, \quad (16)$$

where $F_p(\cdot)$ and $F_q(\cdot)$ is the cumulative distribution functions of $p(\mathbf{z})$ and $q(\mathbf{z})$ respectively.

Recently, the closed-form expression of Wasserstein distance for one-dimensional probability distribution motivates the definition of sliced Wasserstein distances [18]. The key idea behind it is to project (i.e. slice) the high-dimensional distribution into the marginal density and compute the Wasserstein distance with Eq. 16. The projection process is performed via the Radon transform:

$$\mathcal{R}_p(t; u) = \int_{\mathcal{Z}} p(\mathbf{z}) \delta(t - u \cdot \mathbf{z}) d\mathbf{z}, \forall u \in \mathbb{S}^{M-1}, \forall t \in \mathbb{R}, \quad (17)$$

where \mathbb{S}^{M-1} stands for the M -dimensional unit sphere and $\delta(\cdot)$ denotes the one-dimensional Dirac delta function. Therefore, for a fixed projection $u \in \mathbb{S}^{M-1}$, $\mathcal{R}_p(\cdot; u)$, $\mathcal{R}_q(\cdot; u)$ is a one-dimensional slice of density $p(\mathbf{z})$, $q(\mathbf{z})$, respectively. However, one random projection is insufficient to capture all the topology information. [18] leverages a set of slicing ($\{u_1, \dots, u_L\}$) and then averages them:

$$\mathcal{L}_{SW} = \sum_{i=1}^L W_1(\mathcal{R}_p(\cdot; u^{(i)}), \mathcal{R}_q(\cdot; u^{(i)})). \quad (18)$$

Algorithm 2: The PSW autoencoder based anomaly detection

Target:

Learn a network for modelling the distribution of input \mathbf{x} , which can well reconstruct the normal data \mathbf{x}_{nor} but the anomaly \mathbf{x}_{ano} ;

Procedure:

Step 1: Initialize networks $f_\varphi(\cdot)$, $f_\theta(\cdot)$;

Step 2: **while** not converged **do**

- 1: Randomly sample the normal data: $\mathbf{x} \sim p_{gt}(\mathbf{x})$;
- 2: Encode each data with its latent features: $\mathbf{z} = f_\varphi(\mathbf{x})$;
- 3: Construct the kernel: $\mathbf{K} = \Phi(\mathbf{Z})^T \Phi(\mathbf{Z})$;
- 4: Eigen-decomposition of the kernel matrix via the Eq. 22;
- 5: Compute the projection matrix: $\mathbf{U} = \mathbf{K}_c \mathbf{V} \Sigma^{-1}$, and select the first eigenvector $u^{(F)} = \mathbf{U}_1$;
- 6: Sample $\tilde{\mathbf{z}}$ from the prior: $\tilde{\mathbf{z}} \sim p(\mathbf{z})$;
- 7: Sort $u^{(F)} \cdot \mathbf{z}$ such that $u^{(F)} \cdot z_{[m-1]} \leq u^{(F)} \cdot z_{[m]}$;
- 8: Sort $u^{(F)} \cdot \tilde{\mathbf{z}}$ such that $u^{(F)} \cdot \tilde{z}_{[m-1]} \leq u^{(F)} \cdot \tilde{z}_{[m]}$;
- 9: Calculate the Wasserstein distance \mathcal{L}_{PSW} via Eq. 24
- 10: Generate (reconstruct) the input data: $\hat{\mathbf{x}} = f_\theta(\mathbf{z})$;
- 11: Calculate the reconstruction error: $\mathcal{L}_{rec} = \|\hat{\mathbf{x}} - \mathbf{x}\|_2^2$;
- 12: Δ Updates $f_\varphi(\cdot)$ and $f_\theta(\cdot)$ with $\mathcal{L}_{rec} + \mathcal{L}_{PSW}$;

end while

Step 3: Calculate the reconstruction error of test data: \mathcal{L}_{rec}^{Test} ;

Step 4: Set a threshold ϵ : $\hat{y}_{ano} = \{\mathcal{L}_{rec}^{Test} \geq \epsilon\}$;

Output: The best anomaly detection accuracy;

The parameter of networks $f_\varphi(\cdot)$, $f_\theta(\cdot)$.

Although a large number of L can mitigate the uncertainty of the Radon transform, the high computational cost, and the linear assumption pose challenges.

In this paper, we propose the projected sliced Wasserstein to deal with these problems. The intuitive idea of projection (i.e. slicing) is to find the principal component of the latent codes, which can done by the eigen-decomposition on the data, directly. Moreover, considering the non-linearity of the latent features, we leverage the kernel trick:

$$\Phi : \mathcal{Z} \mapsto \mathcal{H}. \quad (19)$$

Thus, we firstly construct the kernel matrix:

$$\mathbf{K} = \Phi(\mathbf{Z})^T \Phi(\mathbf{Z}) \in \mathbb{R}^{n \times n}, \quad (20)$$

where n is the number of batch size. The centered kernel matrix is performed:

$$\begin{aligned} \mathbf{K}_c &= \mathbf{K} - \mathbf{1}_n \mathbf{K} - \mathbf{K} \mathbf{1}_n + \mathbf{1}_n \mathbf{K} \mathbf{1}_n \\ &= (\mathbf{I} - \mathbf{1}_n) \mathbf{K} (\mathbf{I} - \mathbf{1}_n), \end{aligned} \quad (21)$$

where $\mathbf{1}_n$ is a $n \times n$ matrix with all elements equal to $\frac{1}{n}$. Then, we perform a stable eigen-decomposition method of the centered kernel matrix. Motivated by the [20], the singular value decomposition (SVD) is leveraged in the forward pass for initialization purposes $\mathbf{V} \Sigma \mathbf{V}^T = \text{svd}(\mathbf{K}_c)$, then the gradient is computed for back-propagation from the Power Iteration (PI) method [20]. PI compute the leading eigenvector of \mathbf{K}_c based on the iterative update:

$$\mathbf{v}^{(k)} = \frac{\mathbf{K}_c \mathbf{v}^{(k-1)}}{\|\mathbf{K}_c \mathbf{v}^{(k-1)}\|_2}, \quad (22)$$

in which the initial leading eigenvector is computed by the SVD (i.e. $\mathbf{K}_c \approx \mathbf{v}^{(0)} \lambda^{(0)} \mathbf{v}^{(0)T}$), not a random vectors. Then the eigen-decomposition gradients can be calculated as [20]:

$$\begin{aligned} \frac{\partial L}{\partial \mathbf{K}_c} &= \sum_{k=0}^{K-1} \frac{(\mathbf{I} - \mathbf{v}^{(k+1)} \mathbf{v}^{(k+1)T})}{\|\mathbf{K}_c \mathbf{v}^{(k)}\|_2} \frac{\partial L}{\partial \mathbf{v}^{(k)}} \mathbf{v}^{(k)T}, \\ \frac{\partial L}{\partial \mathbf{v}^{(k)}} &= \mathbf{K}_c \frac{(\mathbf{I} - \mathbf{v}^{(k+1)} \mathbf{v}^{(k+1)T})}{\|\mathbf{K}_c \mathbf{v}^{(k)}\|_2} \frac{\partial L}{\partial \mathbf{v}^{(k+1)}}, \end{aligned} \quad (23)$$

where L is the loss function, K means the number of iteration. Based on these gradients, the back-propagation optimization is more stable and not oscillating. In the end, the projection matrix can be computed with $\mathbf{U} = \mathbf{K}_c \mathbf{V} \Sigma^{-1}$. We utilize the leading eigenvector $u^{(F)}$ for slicing the high-dimensional latent data into one-dimension. The proposed projected sliced Wasserstein distances can be formulated as:

$$\mathcal{L}_{PSW} = W_1(\mathcal{RP}_p(\cdot; u^{(F)}), \mathcal{RP}_q(\cdot; u^{(F)})), \quad (24)$$

where

$$\begin{aligned} \mathcal{RP}_p(t; u^{(F)}) &= \int_{\mathbf{Z}} p(\mathbf{z}) \delta(t - u^{(F)} \cdot \mathbf{z}) d\mathbf{z}, \forall t \in \mathbb{R}, \\ \mathcal{RP}_q(t; u^{(F)}) &= \int_{\mathbf{Z}} q(\mathbf{z}|\mathbf{x}) \delta(t - u^{(F)} \cdot \mathbf{z}) d\mathbf{z}, \forall t \in \mathbb{R}. \end{aligned} \quad (25)$$

Compared with the sliced Wasserstein distances (Eq. 18), the proposed distance can be more computation efficient and less uncertain. Finally, the autoencoder network is optimized with:

$$\mathcal{L} = \mathcal{L}_{rec} + \lambda \mathcal{L}_{PSW}, \quad (26)$$

where λ is the hyperparameter.

IV. EXPERIMENTS AND RESULTS ANALYSIS

In this section, we illustrate the performance of the proposed projected sliced Wasserstein autoencoder for hyperspectral anomaly detection by experiments and compared with some existing algorithms. All experiments are tested on a computer with Intel Core i7 CPU @ 2.50 GHz, NVIDIA GeForce RTX 3060 under Windows 10 Professional.

A. Experiments on the Blood Detection Hyperspectral Data

We conduct experiments on the hyperspectral images datasets for blood detection [42]. In particular, we select four scenarios, named $A(1)$, $B(1)$, $C(1)$, $D(1)$, as shown in Fig. 3. The blood, annotated as label one, is viewed as the anomaly data. **Scene A ‘Head’**: The blood is located on white materials, i.e. bandage, white sheet, on the left side of the blue shirt. The near background of the blood traces is fairly uniform, yet the far of the image is a mixture of substances, including fruits and vegetables with different colors. In addition, there are traces of real and artificial blood, which is the main challenge. **Scene B ‘Shirt’**: Traces of real and artificial blood are located on the blue material of the cotton shirt. This scene allows examining the effectiveness of blood detection on a dark background. **Scene C ‘Knife’**: In this scenario, traces of blood are present on the blade and handle of the knife and in its vicinity. **Scene D ‘Splash’**: This scene includes a blood splash pattern on a white cotton shirt. All hyperspectral data acquisition is performed

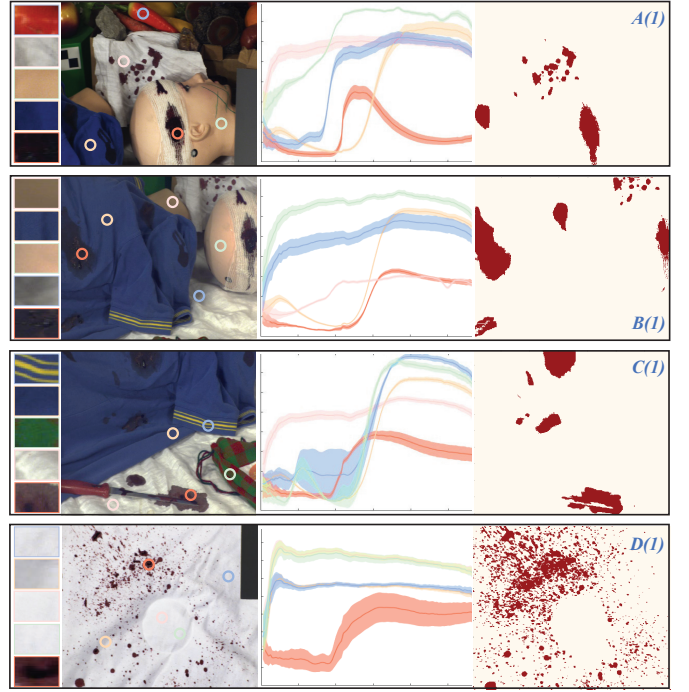


Fig. 3: The visualization of the RGB images, label map, and the hyperspectral spectrum of samples. The areas in the blue, pink, green, and orange ring are normal (background) samples with different materials. The anomaly (blood) samples are shown in the red ring.

with Surface Optics SOC710 camera, which ranges from 377 to 1046 nm. The dimensions of the output image are 696×520 with 113 bands ($B = 113$) and a 12-bit dynamic range. More details about the lighting, reflectance correction, and dataset annotation can be seen in [42].

Firstly, we conduct experiments of the β -VAE based anomaly detection on four hyperspectral blood datasets. We would like to verify the assumption that the KL divergence is a strong notion of regularization. The encoder network of the β -VAE is built by three fully connected layers and non-linear activation layers (i.e. ReLU). In particular, the dimension of the encoder network output is 16 ($M = 16$). The architecture of the decoder network is the inverse of the encoder. The dimension of the decoder output is 113 ($B = 113$). The performance and result of the β -VAE with $\beta > 0.1$ (i.e. $-\log \beta < 1$) is not reported, since the reconstruction error of normal samples and outliers are mixed that cannot give an useful classification. From the first row of Fig. 4, we can observe that the performance, including Kappa, Recall, Precision, F1-score, and the area under the ROC curve (AUC) is highly sensitive to the β . For example, the Kappa coefficient of the β -VAE on $A(1)$ is 11.45 when the $-\log \beta = 1$, while 63.83 when $-\log \beta = 4$. Similarly, the F1-score of the β -VAE on $A(1)$ is 60.98 when the $-\log \beta = 1$, while 82.70 when $-\log \beta = 4$; the AUC of the β -VAE on $D(1)$ is 65.54 when the $-\log \beta = 1$, while 83.13 when $-\log \beta = 4$. Moreover, with an extreme small β (i.e. $-\log \beta = 5$), the performance drops a little for all four dataset.

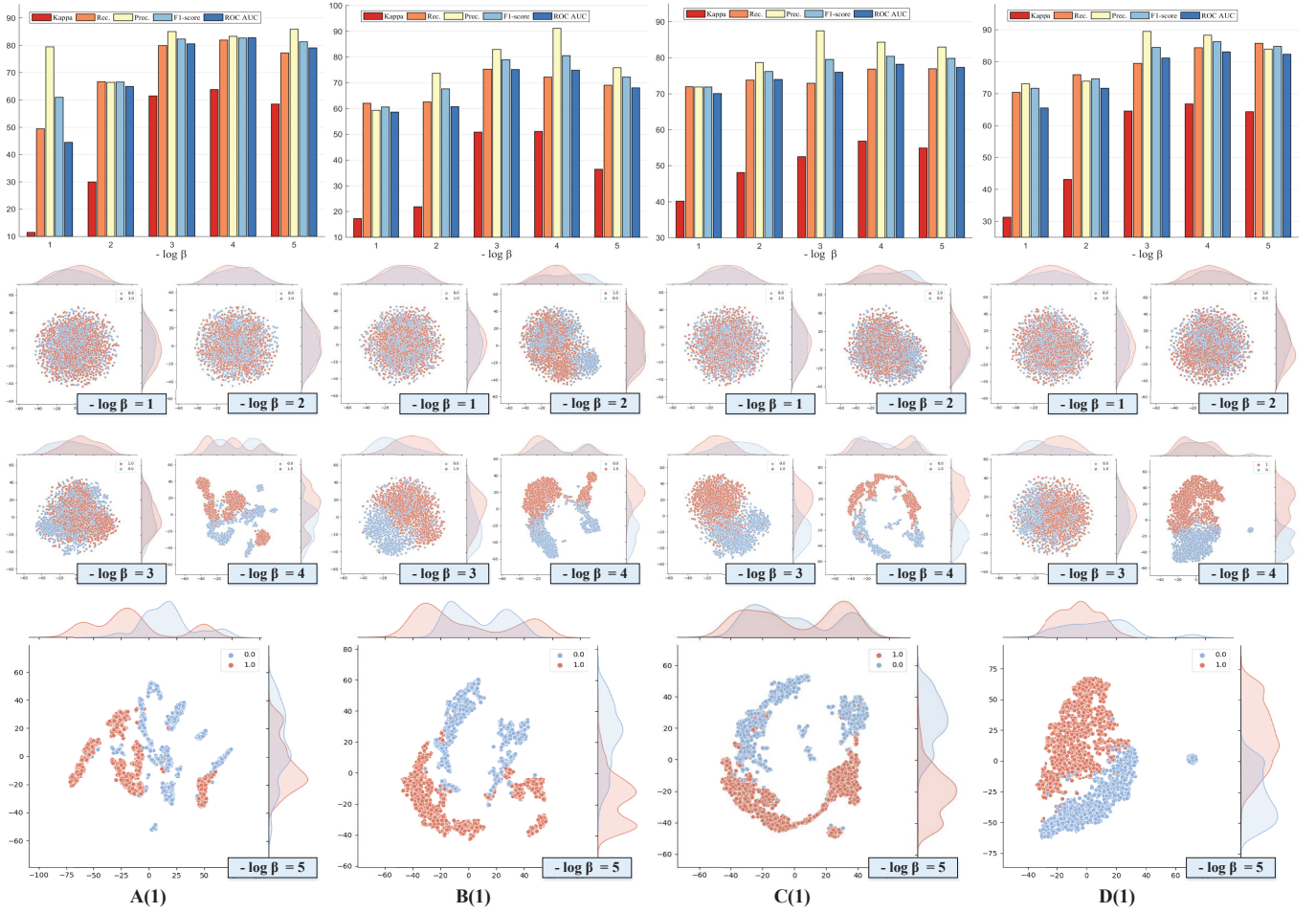


Fig. 4: The performance and t-SNE visualization of the β -VAE on four hyperspectral blood detection datasets. Kappa, Recall (Rec.), Precision (Prec.), F1-score, and AUC are utilized as the performance evaluation metric.

TABLE II: The experiments for the number of slicing, the hyperparameter λ , and different prior distributions of SWAE on A(1) blood detection dataset. Kappa, Recall, Precision, F1-score, and AUC are utilized as evaluation metrics.

| | | λ | | | | | | | | | | | | | | |
|----------|-----------|-----------------------|-----------------|---------------|----------------|-----------------|-------------------------|-----------------|---------------|----------------|-----------------|--------------------------|-----------------|---------------|----------------|-----------------|
| | | Number of slicing = 1 | | | | | Number of slicing = 100 | | | | | Number of slicing = 1000 | | | | |
| Prior | | $\lambda = 0.01$ | $\lambda = 0.1$ | $\lambda = 1$ | $\lambda = 10$ | $\lambda = 100$ | $\lambda = 0.01$ | $\lambda = 0.1$ | $\lambda = 1$ | $\lambda = 10$ | $\lambda = 100$ | $\lambda = 0.01$ | $\lambda = 0.1$ | $\lambda = 1$ | $\lambda = 10$ | $\lambda = 100$ |
| Gaussian | Kappa | 84.85 | 83.06 | 62.22 | 67.83 | — | 76.29 | 85.03 | 76.91 | 79.19 | 48.11 | 78.96 | 79.91 | 82.58 | 70.96 | 56.23 |
| | Recall | 91.19 | 90.95 | 80.01 | 84.37 | — | 84.96 | 89.71 | 84.83 | 87.53 | 70.93 | 83.73 | 86.84 | 88.43 | 82.08 | 71.36 |
| | Precision | 94.61 | 92.96 | 85.23 | 84.93 | — | 93.95 | 96.72 | 95.12 | 93.48 | 84.88 | 95.87 | 95.07 | 96.09 | 96.03 | 97.09 |
| | F1-score | 92.87 | 91.95 | 82.54 | 84.65 | — | 89.11 | 93.08 | 89.08 | 90.41 | 77.28 | 90.51 | 90.77 | 92.10 | 87.33 | 82.27 |
| | AUC | 92.24 | 91.77 | 81.02 | 85.77 | — | 87.70 | 91.72 | 88.23 | 81.60 | 73.56 | 89.82 | 89.68 | 91.10 | 86.08 | 77.62 |
| Ring | Kappa | 83.44 | 76.38 | 76.34 | 54.46 | — | 74.41 | 77.09 | 74.17 | 57.83 | 29.03 | 81.33 | 76.15 | 67.40 | 64.78 | 42.94 |
| | Recall | 90.42 | 86.42 | 86.41 | 72.62 | — | 84.19 | 86.15 | 86.06 | 74.05 | 60.58 | 89.02 | 85.28 | 79.98 | 78.72 | 69.04 |
| | Precision | 94.15 | 91.96 | 91.96 | 91.05 | — | 93.21 | 92.96 | 90.08 | 93.43 | 95.57 | 93.64 | 93.38 | 92.15 | 91.18 | 83.33 |
| | F1-score | 92.15 | 89.10 | 89.11 | 80.80 | — | 88.47 | 89.42 | 88.02 | 82.14 | 74.16 | 91.27 | 89.15 | 85.04 | 84.50 | 75.52 |
| | AUC | 91.78 | 88.08 | 88.07 | 75.07 | — | 87.01 | 88.99 | 87.07 | 78.22 | 64.35 | 90.57 | 88.04 | 83.67 | 81.37 | 70.12 |
| Moons | Kappa | 82.83 | 79.54 | 64.95 | 60.69 | 35.10 | 79.67 | 83.66 | 77.06 | 54.84 | 47.73 | 82.66 | 78.62 | 79.91 | 17.57 | 51.37 |
| | Recall | 89.38 | 89.74 | 79.76 | 76.85 | 64.68 | 87.87 | 92.29 | 86.91 | 73.49 | 72.74 | 90.43 | 87.77 | 88.07 | 57.45 | 71.21 |
| | Precision | 94.80 | 90.94 | 89.25 | 90.42 | 86.75 | 93.72 | 92.20 | 92.19 | 89.67 | 81.18 | 93.14 | 92.41 | 93.47 | 96.02 | 86.24 |
| | F1-score | 92.01 | 90.33 | 84.24 | 83.09 | 74.10 | 90.69 | 92.25 | 89.47 | 80.77 | 76.73 | 91.76 | 90.32 | 90.69 | 71.89 | 78.01 |
| | AUC | 91.06 | 90.01 | 82.31 | 80.59 | 70.06 | 89.77 | 91.98 | 88.34 | 76.73 | 73.06 | 91.29 | 89.22 | 89.85 | 58.45 | 75.69 |

— represents that the value is too small that the model cannot classify the anomaly.

To figure out the reason why the result is highly unstable to the β , we visualize the distribution of learned latent features via t-SNE [43]. We can see that the distribution of latent is less like Gaussian when decreasing the β ($-\log \beta = 1$ to 5).

Note that we only modelling the normal samples (the blue points), we would like to approximate the latent feature of them to the prior while the latent codes of anomalies do not follow the prior distribution. With a fairly large β ($-\log \beta = 1$

TABLE III: Summary of model anomaly detection performance on four hyperspectral blood detection datasets. Kappa, Recall, Precision, F1-score, and AUC are utilized as evaluation metrics.

| Method | | PCA | OCSVM | COPOD | IForest | LODA | FastABOD | AvgKNN | LOF | β -VAE | l_2 -AE | SWAE | PSWAE (Ours) |
|---------|-----------|-------|-------|-------|---------|-------|----------|--------|--------------|-----------------------------------|-----------------|-----------------------------------|-----------------------------------|
| Dataset | | | | | | | | | | | | | |
| Scene A | Kappa | - | - | - | - | 01.48 | 31.01 | 40.49 | 39.98 | 63.83 \pm 0.3 | 75.10 \pm 0.2 | 84.85 \pm 0.2 | 88.81 \pm 0.2 |
| | Recall | - | - | - | - | 09.34 | 23.98 | 29.79 | 29.06 | 82.03 \pm 0.2 | 87.51 \pm 0.3 | 91.19 \pm 0.3 | 92.28 \pm 0.1 |
| | Precision | - | - | - | - | 11.37 | 68.31 | 86.99 | 90.24 | 83.38 \pm 0.4 | 87.60 \pm 0.4 | 94.61 \pm 0.3 | 96.90 \pm 0.2 |
| | F1-score | - | - | - | - | 10.25 | 34.49 | 44.38 | 43.96 | 82.70 \pm 0.3 | 87.56 \pm 0.4 | 92.87 \pm 0.3 | 94.54 \pm 0.1 |
| | AUC | - | - | - | - | 50.81 | 79.19 | 88.79 | 90.07 | 81.89 \pm 0.2 | 88.34 \pm 0.3 | 92.24 \pm 0.2 | 94.40 \pm 0.1 |
| Scene B | Kappa | 05.63 | 07.39 | 08.43 | 10.40 | 02.74 | 10.96 | 16.81 | 43.27 | 51.06 \pm 0.3 | 42.94 \pm 0.4 | 75.25 \pm 0.2 | 79.50 \pm 0.1 |
| | Recall | 12.66 | 14.05 | 14.82 | 16.28 | 10.34 | 16.73 | 20.89 | 37.67 | 72.21 \pm 0.3 | 71.37 \pm 0.2 | 88.77 \pm 0.3 | 90.44 \pm 0.2 |
| | Precision | 16.57 | 18.29 | 19.66 | 22.22 | 13.04 | 22.76 | 30.61 | 71.25 | 91.12 \pm 0.4 | 80.17 \pm 0.3 | 88.45 \pm 0.2 | 88.90 \pm 0.1 |
| | F1-score | 14.23 | 15.89 | 16.90 | 18.79 | 11.54 | 19.29 | 24.83 | 49.29 | 80.57 \pm 0.3 | 75.51 \pm 0.3 | 88.61 \pm 0.3 | 89.66 \pm 0.2 |
| | AUC | 53.18 | 54.21 | 54.84 | 56.06 | 51.53 | 56.38 | 60.19 | 80.42 | 74.94 \pm 0.2 | 71.25 \pm 0.2 | 87.63 \pm 0.2 | 89.75 \pm 0.1 |
| Scene C | Kappa | 27.59 | 18.41 | 23.25 | 34.59 | 43.57 | 31.04 | 36.84 | 45.06 | 56.81 \pm 0.4 | 46.86 \pm 0.2 | 73.32 \pm 0.2 | 73.90 \pm 0.2 |
| | Recall | 24.50 | 18.65 | 22.55 | 28.72 | 49.40 | 26.91 | 30.62 | 34.67 | 76.89 \pm 0.4 | 70.14 \pm 0.3 | 86.65 \pm 0.3 | 86.19 \pm 0.2 |
| | Precision | 52.38 | 36.90 | 40.86 | 65.50 | 55.88 | 56.88 | 66.39 | 87.67 | 84.32 \pm 0.5 | 87.96 \pm 0.1 | 88.15 \pm 0.2 | 88.00 \pm 0.1 |
| | F1-score | 33.39 | 24.78 | 29.06 | 39.93 | 52.44 | 36.54 | 41.19 | 49.69 | 80.44 \pm 0.4 | 78.05 \pm 0.2 | 87.39 \pm 0.2 | 87.79 \pm 0.2 |
| | AUC | 71.15 | 63.23 | 66.05 | 77.68 | 72.97 | 73.62 | 78.51 | 88.68 | 74.94 \pm 0.3 | 73.08 \pm 0.2 | 86.63 \pm 0.1 | 86.95 \pm 0.2 |
| Scene D | Kappa | 30.79 | 31.10 | 18.34 | 38.53 | 55.49 | 59.44 | 64.62 | 64.85 | 66.81 \pm 0.2 | 45.09 \pm 0.2 | 65.28 \pm 0.3 | 74.98 \pm 0.2 |
| | Recall | 41.20 | 41.68 | 34.82 | 46.59 | 55.72 | 57.28 | 59.96 | 59.68 | 84.36 \pm 0.1 | 77.33 \pm 0.4 | 85.68 \pm 0.2 | 85.50 \pm 0.3 |
| | Precision | 40.76 | 41.04 | 23.56 | 49.24 | 72.30 | 78.99 | 86.46 | 87.72 | 88.33 \pm 0.2 | 75.93 \pm 0.2 | 83.87 \pm 0.4 | 90.25 \pm 0.1 |
| | F1-score | 40.98 | 41.26 | 28.10 | 47.88 | 62.94 | 66.40 | 70.81 | 71.05 | 86.29 \pm 0.2 | 76.62 \pm 0.4 | 84.77 \pm 0.2 | 87.79 \pm 0.2 |
| | AUC | 65.32 | 65.49 | 57.95 | 69.72 | 81.16 | 84.38 | 88.21 | 88.73 | 83.13 \pm 0.3 | 72.62 \pm 0.3 | 84.77 \pm 0.3 | 87.45 \pm 0.3 |

- represents that the value is too small that the model cannot classify the anomaly.

TABLE IV: The ablation experiments for the hyperparameter λ , and different prior distributions of proposed PSWAE on $A(I)$ blood detection dataset.

| λ | | $\lambda = 0.01$ | $\lambda = 0.1$ | $\lambda = 1$ | $\lambda = 10$ | $\lambda = 100$ |
|-----------|-----------|------------------|-----------------|---------------|----------------|-----------------|
| Prior | | | | | | |
| Gaussian | Kappa | 81.50 | 79.80 | 82.30 | 73.70 | 54.09 |
| | Recall | 88.77 | 85.88 | 88.57 | 82.13 | 70.83 |
| | Precision | 93.30 | 95.50 | 94.50 | 94.30 | 92.00 |
| | F1-score | 90.98 | 90.44 | 91.44 | 87.75 | 80.04 |
| | AUC | 90.75 | 89.60 | 92.09 | 86.43 | 77.90 |
| Ring | Kappa | 76.17 | 80.00 | 79.50 | 60.40 | 40.80 |
| | Recall | 85.87 | 86.20 | 85.21 | 74.43 | 64.82 |
| | Precision | 92.93 | 96.83 | 96.23 | 92.00 | 89.20 |
| | F1-score | 89.07 | 91.18 | 90.37 | 82.29 | 75.08 |
| | AUC | 88.18 | 89.50 | 90.45 | 81.34 | 70.40 |
| Moons | Kappa | 88.80 | 73.80 | 79.80 | 73.75 | 56.90 |
| | Recall | 92.28 | 84.05 | 85.82 | 83.88 | 73.63 |
| | Precision | 96.90 | 91.10 | 95.60 | 91.35 | 93.80 |
| | F1-score | 94.54 | 87.43 | 90.44 | 87.45 | 81.59 |
| | AUC | 94.40 | 87.50 | 92.05 | 88.38 | 79.25 |

and 2), however, both the latent variable \mathbf{z} of the normal data (blue point) and the outlier (red point) perfectly follows the standard Gaussian prior. When decreasing the β to $-\log \beta = 3$, the distribution can maintain the Gaussian characteristic and be easily separated. Moreover, when $-\log \beta = 5$, the KL only serves a little regularization. Therefore, the distribution of latent code is similar to the manifold of the data.

In conclusion, it is clear that the KL divergence always provides useless constraints when performing the VAE on anomaly detection. Only with a small β (i.e. a weak optimization for the KL divergence and a good optimization for

reconstruction loss), the VAE can be used to perform anomaly detection. However, β needs adjust for each dataset.

Then, we provide the anomaly detection performance result of the Sliced Wasserstein autoencoder (SWAE) on $A(I)$ dataset. Similar to the β -VAE, the architecture of SWAE is also built by the combination of the fully connected layer and ReLU. But the dimension of the feature is 2 ($M = 2$). We firstly conduct experiments for the number of slicing (L in Eq. 18). The number of slicing ranges from 1 to 1000. We can observe that the number of slicing has an effect on the performance. As shown in Table II, under the $\lambda = 1$ and the Gaussian prior, the Kappa coefficient is 62.22 when $L = 1$ and 82.58 when $L = 1000$. Yet, the performance is not correlated with the number of slicing. For example, the performance of $L = 100$ is better than $L = 1000$ under the $\lambda = 10$ and the Gaussian prior, and so on. This result verifies the SWAE is unstable to the number of slicing, due to this process being stochastic. In addition, we assign different prior distributions, such as ring and moons¹. However, in most cases, the performance of the model with these complex priors is inferior to the Gaussian. This is because the linear projection, used by SWAE, may result in collapse when the data space is the non-linear manifold.

In the end, we compare the proposed projected sliced Wasserstein autoencoder (PSWAE) with existing methods on four hyperspectral blood detection datasets. The network architecture is the same as the SWAE. The number of power iteration K is 10. Baseline methods, including PCA [22], OCSVM [37], COPOD [38], IForest [28], LODA [44], FastABOD [30], AvgKNN [31], LOF [29], are implemented via the PyOD

¹Generate the ring-like and moons-like data via the sklearn library: <https://scikit-learn.org/stable/modules/classes.html>

TABLE V: Summary of model anomaly detection performance on seven hyperspectral vaccine anomaly detection datasets. AUC is utilized as the evaluation metrics.

| Method \ Dataset | Local RX | CRD | Global RX | DWT RX | PSWAE (Ours) |
|------------------|----------|-------|---------------|--------|---------------|
| Case 1 | 52.47 | 83.02 | 99.99 | 99.99 | 100.00 |
| Case 2 | 52.10 | 91.77 | 100.00 | 99.99 | 100.00 |
| Case 3 | 54.55 | 92.09 | 99.99 | 99.99 | 100.00 |
| Case 4 | 51.68 | 84.43 | 99.96 | 99.96 | 99.98 |
| Case 5 | 52.44 | 95.73 | 99.99 | 99.95 | 99.99 |
| Case 6 | 53.08 | 92.58 | 99.98 | 99.98 | 99.99 |
| Case 7 | 52.88 | 99.59 | 99.95 | 99.95 | 99.98 |

library [45]. β -VAE, l_2 -AE, SWAE, and our proposed algorithm are implemented via the Pytorch library. As shown in Table III, the traditional anomaly detection algorithms (PCA, OCSVM, COPOD, IForest, LODA) have a poor performance. Moreover, some classical hyperspectral AD methods are not reported due to their poor scalable and performance. We will conduct them on another benchmark dataset. Ours PSWAE outperforms a lot than the learning-based methods (i.e. β -VAE, l_2 -AE, SWAE). For example, on the $A(I)$ dataset, it boosts the Kappa coefficient by 24.98% compared with the β -VAE, 13.71% compared with l_2 -AE, and 3.98% compared with SWAE. On the $C(I)$ dataset, PSWAE improves by the AUC by 12.01% compared with the β -VAE, 13.87% compared with l_2 -AE, and 0.32% compared with SWAE.

Ablation experiments. We test different prior distributions and the hyperparameter λ . The result is reported in Table IV. Compared with the performance SWAE (as shown in Table II), the proposed projected sliced Wasserstein has less uncertainty. Moreover, our proposed method can improve the model performance when using a more complex distribution. Apart from a large λ (i.e. $\lambda = 100$), the Kappa, Recall, Precision, and AUC of the proposed model are robust to the hyperparameter variation. $\lambda = 100$ (the strong regularization) has an adverse effect on outlier detection is also proofed. In other words, a weak regularization is better for the autoencoder-based anomaly detection, which can push the network to keep more data manifold.

B. Experiments on the Vaccine Anomaly Hyperspectral Data

We also conduct experiments on the hyperspectral vaccine anomaly detection datasets ² to test the generalized capability. The whole dataset consists of seven different hyperspectral images (case 1 - case 7). All data acquisition is performed with CCD camera based on liquid crystal tunable filter (LCTF), which ranges from 400 - 1000 nm. The full width at half maximum (FWHM) is 10nm. The dimension of the hyperspectral image is 680×240 with 101 bands. Compared with the blood detection datasets, this anomaly detection benchmark is easier.

We compare the proposed PSWAE with the classical hyperspectral anomaly detection methods, including Local RX [35], CRD [23], Global RX [33], and DWT RX [36]. The AUC is used as the performance metric. As shown in Table V, our

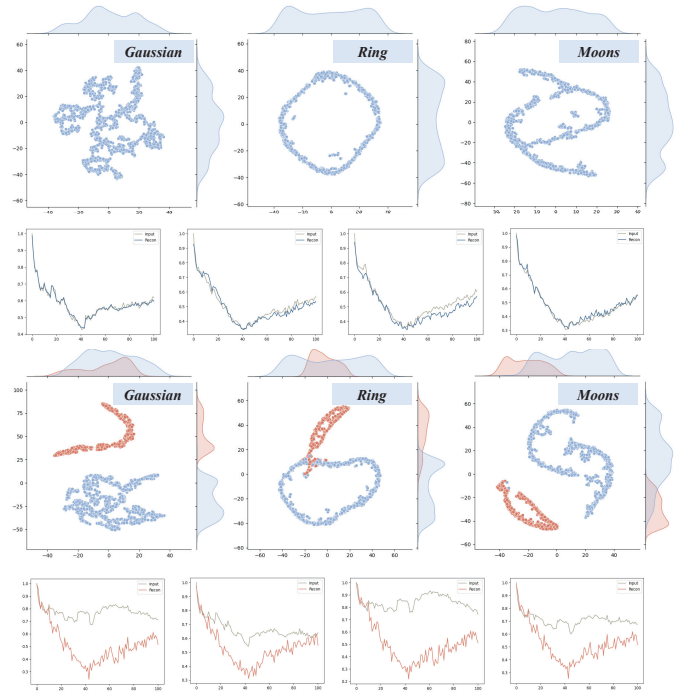


Fig. 5: The t-SNE visualization of the learned latent distribution of the proposed network with different priors, and the visualization of the input and reconstruction spectrum.

algorithm achieves a superior detection result and outperforms all baselines. In addition, we visualize the posterior distribution of the learned latent feature in Fig. 5. These visualization results are conducted on the case 1 dataset. We can observe that the distribution of the normal data is well approximated to the prior. Meanwhile, the distribution of the outlier (red point) is distinct from the blue one. Furthermore, from the input and reconstruction spectrum curve, we can see that the normal data can be reconstructed well but the spectrum of the outlier cannot be reconstructed. The reconstruction of the anomaly is similar to the normal pattern, which is a satisfactory result.

V. CONCLUSION

In this paper, we heuristically investigate the generative model-based anomaly detection on hyperspectral images. Empirically, we conduct experiments for the β -VAE based anomaly detection. We find that the regularization term (i.e. KL divergence) is always too strong for the AD. We change the β to verify the regularization effect. Only with an elaborated weight ($-\log \beta \geq 3$), the VAE can be used to perform outlier detection. In this case, we assume that the neural network achieves a trade-off between learning the data manifold and approximating the prior distribution. However, it is not worth considering to sophisticatedly tune the hyperparameter. Therefore, we introduce the sliced Wasserstein autoencoder for AD. The sliced Wasserstein distance is a weaker notion, compared with KL divergence. Under this framework, we propose a projected sliced Wasserstein distance to deal with the unstable performance and the non-linear measure problem. The designed PSW distance is allowed to calculate as the

²<https://github.com/YurongChen1998/HVAD-Hyperspectral-Vaccine-Anomaly-Detection-dataset>

closed-form. Comprehensive experiments, including blood detection and vaccine outlier detection, demonstrate the superior performance of our method.

REFERENCES

- [1] F. Y. Edgeworth, "On discordant observations," *The London, Edinburgh, and Dublin Philosophical Magazine and Journal of Science*, vol. 23, no. 5, pp. 364–375, 1887.
- [2] S. Li, K. Zhang, P. Duan and X. Kang, "Hyperspectral Anomaly Detection With Kernel Isolation Forest," in *IEEE Transactions on Geoscience and Remote Sensing*, vol. 58, no. 1, pp. 319–329, 2020.
- [3] P. Bergmann, K. Batzner, M. Fauser, D. Sattlegger, and C. Steger, "The MVTec anomaly detection dataset: a comprehensive real-world dataset for unsupervised anomaly detection," in *International Journal of Computer Vision*, vol. 129, pp. 1038–1059, 2021.
- [4] P. Stern, "Perception of dangerous animals," *Science*, vol. 352, no. 6290, pp. 1186–1187, 2016.
- [5] Y. Yuan, D. Ma and Q. Wang, "Hyperspectral anomaly detection by graph pixel selection," in *IEEE Transactions on Cybernetics*, vol. 46, no. 12, pp. 3123–3134, Dec. 2016.
- [6] P. Perera and V. M. Patel, "Learning deep features for one-class classification," in *IEEE Transactions on Image Processing*, vol. 28, no. 11, pp. 5450–5463, 2019.
- [7] P. Oza and V. M. Patel, "One-class convolutional neural network," in *IEEE Signal Processing Letters*, vol. 26, no. 2, pp. 277–281, 2019.
- [8] P. Wu, J. Liu and F. Shen, "A deep one-class neural network for anomalous event detection in complex scenes," in *IEEE Transactions on Neural Networks and Learning Systems*, vol. 31, no. 7, pp. 2609–2622, 2020.
- [9] C. Zhou and R. C. Paffenroth, "Anomaly detection with robust deep autoencoders," in *ACM SIGKDD Conference on Knowledge Discovery and Data Mining*, pp. 665–674, 2017.
- [10] C. Zhao, X. Li, and H. Zhu, "Hyperspectral anomaly detection based on stacked denoising autoencoders," *Journal of Applied Remote Sensing*, vol. 11, no. 4, Sep. 2017.
- [11] X. Lu, W. Zhang and J. Huang, "Exploiting embedding manifold of autoencoders for hyperspectral anomaly detection," in *IEEE Transactions on Geoscience and Remote Sensing*, vol. 58, no. 3, pp. 1527–1537, Mar. 2020.
- [12] S. Wang, X. Wang, L. Zhang and Y. Zhong, "Auto-AD: Autonomous hyperspectral anomaly detection network based on fully convolutional autoencoder," in *IEEE Transactions on Geoscience and Remote Sensing*, doi: 10.1109/TGRS.2021.3057721.
- [13] D. Gong, L. Liu, V. Le, et al., "Memorizing normality to detect anomaly: Memory-augmented deep autoencoder for unsupervised anomaly detection," in *International Conference on Computer Vision (ICCV)*, 2019, pp. 1705–1714.
- [14] J. An, and S. Cho, "Variational autoencoder based anomaly detection using reconstruction probability," *Special Lecture on IE*, vol. 2, no. 1, pp. 1–18, 2015.
- [15] D. P. Kingma, and M. Welling, "Auto-encoding variational bayes," in *International Conference on Learning Representations (ICLR)*, 2014.
- [16] I. Tolstikhin, O. Bousquet, S. Gelly, B. Schoelkopf, "Wasserstein Auto-Encoders," in *International Conference on Learning Representations (ICLR)*, 2018.
- [17] M. D. Hoffman, M. J. Johnson, "Elbo surgery: yet another way to carve up the variational evidence lower bound," in *Workshop in Advances in Approximate Bayesian Inference*, 2016.
- [18] S. Kolouri, G. Rohde, H. Hoffmann, "Sliced wasserstein distance for learning Gaussian mixture models," in *Computer Vision and Pattern Recognition (CVPR)*, 2018: 3427–3436.
- [19] I. Higgins, L. Matthey, A. Pal, et al., "beta-vae: Learning basic visual concepts with a constrained variational framework," in *International Conference on Learning Representations (ICLR)*, 2017.
- [20] W. Wei, D. Zheng, H. Yinlin, F. Pascal, S. Mathieu, "Backpropagation-friendly eigendecomposition," in *Advances in Neural Information Processing Systems (NeurIPS)*, 2019.
- [21] M. Johnson, D. K. Duvenaud, A. Wiltchko, R. P. Adams, and S. R. Datta, "Composing graphical models with neural networks for structured representations and fast inference," in *Advances in Neural Information Processing Systems (NeurIPS)*, pp. 2946–2954, 2016.
- [22] Q. Ding and E. D. Kolaczyk, "A compressed PCA subspace method for anomaly detection in high-dimensional data," in *IEEE Transactions on Information Theory*, vol. 59, no. 11, pp. 7419–7433, Nov. 2013.
- [23] W. Li and Q. Du, "Collaborative representation for hyperspectral anomaly detection," in *IEEE Transactions on Geoscience and Remote Sensing*, vol. 53, no. 3, pp. 1463–1474, Mar. 2015.
- [24] S. Yang and Z. Shi, "Hyperspectral image target detection improvement based on total variation," in *IEEE Transactions on Image Processing*, vol. 25, no. 5, pp. 2249–2258, 2016.
- [25] S. Huang, B. Cornelis, B. Devolder, M. Martens and A. Pizurica, "Multimodal target detection by sparse coding: application to paint loss detection in paintings," in *IEEE Transactions on Image Processing*, vol. 29, pp. 7681–7696, 2020.
- [26] L. Li, W. Li, Q. Du and R. Tao, "Low-rank and sparse decomposition with mixture of Gaussian for hyperspectral anomaly detection," in *IEEE Transactions on Cybernetics*, vol. 51, no. 9, pp. 4363–4372, Sept. 2021.
- [27] H. Zhu, H. Ni, S. Liu, G. Xu and L. Deng, "TNLRS: Target-aware non-Local low-rank modeling with saliency filtering regularization for infrared small target detection," in *IEEE Transactions on Image Processing*, vol. 29, pp. 9546–9558, 2020.
- [28] L. Tony, T. Ming, Z. Hua, "Isolation forest," in *Proceedings of the IEEE International Conference on Data Mining (ICDM)*, 2008, pp. 413–422.
- [29] M. Breunig, H. Kriegel, T. Raymond, and J. Sander, "Lof: identifying density-based local outliers," in *ACM sigmod record*, vol. 29, pp. 93–104, 2000.
- [30] H. Kriegel, M. Schubert, A. Zimek, "Angle-based outlier detection in high-dimensional data," in *Proceedings of the ACM SIGKDD International Conference on Knowledge Discovery and Data Mining*, 2008, pp. 444–452.
- [31] S. Ramaswamy, R. Rastogi, and K. Shim, "Efficient algorithms for mining outliers from large data sets," in *ACM sigmod record*, vol. 29, pp. 427–438, 2000.
- [32] B. Du, Y. Zhang, L. Zhang and D. Tao, "Beyond the Sparsity-Based Target Detector: A hybrid sparsity and statistics-based detector for hyperspectral images," in *IEEE Transactions on Image Processing*, vol. 25, no. 11, pp. 5345–5357, 2016.
- [33] I. S. Reed and X. Yu, "Adaptive multiple-band CFAR detection of an optical pattern with unknown spectral distribution," in *IEEE Transactions on Acoustics, Speech, and Signal Processing*, vol. 38, no. 10, pp. 1760–1770, Oct. 1990.
- [34] Q. Guo, B. Zhang, Q. Ran, L. Gao, J. Li and A. Plaza, "Weighted-RXD and linear filter-based RXD: Improving background statistics estimation for anomaly detection in hyperspectral imagery," in *IEEE Journal of Selected Topics in Applied Earth*, vol. 7, no. 6, pp. 2351–2366, Jun. 2014.
- [35] J. Molero, E. Garzon, I. Garcia, and A. Plaza, "Analysis and optimizations of global and local versions of the RX algorithm for anomaly detection in hyperspectral data," in *IEEE Journal of Selected Topics in Applied Earth Observations and Remote Sensing*, vol. 6, no. 2, pp. 801–814, 2013.
- [36] M. Baghbid, K. Jamshidi, A. Nilchi, S. Homayouni, "Improvement of anomaly detection algorithms in hyperspectral images using discrete wavelet transform," *Signal and Image Processing* vol. 2, no. 4, pp. 13–25, 2011.
- [37] B. Scholkopf, J. Platt, J. Shawe-Taylor, A. Smola, and R. Williamson, "Estimating the support of a high-dimensional distribution," *Neural Computing*, vol. 13, no. 7, pp. 1443–1471, 2001.
- [38] Z. Li, Y. Zhao, N. Botta, et al., "Copula-based outlier detection," in *Proceedings of the IEEE International Conference on Data Mining (ICDM)*, 2020, pp. 17–20.
- [39] X. Cao, F. Zhou, L. Xu, D. Meng, Z. Xu and J. Paisley, "Hyperspectral image classification with markov random fields and a convolutional neural network," in *IEEE Transactions on Image Processing*, vol. 27, no. 5, pp. 2354–2367, 2018.
- [40] D. M. Blei, A. Kucukelbir, J. D. McAuliffe, "Variational inference: A review for statisticians," *Journal of the American statistical Association*, vol. 112, no. 518, pp. 859–877, 2017.
- [41] B. Poole, S. Ozair, A. V. D. Oord, et al., "On variational bounds of mutual information," in *International Conference on Machine Learning (ICML)*, pp. 5171–5180, 2019.
- [42] M. Romaszewski, P. Glomb, A. Sochan, et al., "A dataset for evaluating blood detection in hyperspectral images," *Forensic Science International*, vol. 320, 2021.
- [43] V. Maaten, G. Hinton, "Visualizing data using t-SNE," *Journal of machine learning research*, vol. 9, no. 11, 2008.
- [44] T. Pevn, "Loda: lightweight on-line detector of anomalies," *Machine Learning*, vol. 102, no. 2, pp. 275–304, 2016.
- [45] Z. Yue, N. Zain and L., Zheng, "PyOD: A python toolbox for scalable outlier detection," *Journal of Machine Learning Research*, vol. 20, no. 96, pp. 1–7, 2019.